Journal of Sound and Vibration (1997) **200**(2), 121–137

BIFURCATIONS AND CHAOTIC MOTIONS IN A RATE GYRO WITH A SINUSOIDAL VELOCITY ABOUT THE SPIN AXIS

Z.-M. Ge and H.-H. Chen

Department of Mechanical Engineering, *National Chiao Tung University*, *Hsinchu*, *Taiwan*, *Republic of China*

(*Received* 6 *June* 1995, *and in final form* 15 *March* 1996)

An analysis is presented for a single-axis rate gyro mounted on a space vehicle undergoing sinusoidal motion and steady rotation about its spin and output axes. By varying the amplitude of sinusoidal motion, the periodic and chaotic responses of this parametrically excited non-linear system are investigated using the incremental harmonic balance (IHB) method and numerical integration. The multi-variable Floquet theory is applied to analyze the stability of periodic attractors and the behavior of bifurcations. Additionally, phase portraits, Poincaré maps, average power spectra, bifurcation diagrams, parametric diagrams and Lyapunov exponents are presented to observe Hopf bifurcation, symmetry-breaking bifurcations, period-doubling bifurcations and chaotic motions. The cell mapping technique (MICM) is also used to study the basins of attraction of periodic attractors.

1. INTRODUCTION

A number of studies over the past few decades have shown that chaotic phenomena are observed in many physical systems that possess both non-linearity and external excitation [1, 2]. In a gyroscopic system, a single-axis rate gyro mounted on a space vehicle free to move in various ways also exhibits complex non-linear and chaotic motions. Its stability was broadly characterized into stable regions in which the angular velocity of a given vehicle was measured by Singh and Ge [3, 4]. Here, we further investigate the non-linear nature of a single-axis rate gyro when the vehicle is simultaneously spinning sinusoidally and steadily rotating with respect to the spin and output axes of the gyro. This system is characterized by parametric excitation and exhibits complex non-linear phenomena [1, 5] in the presence of sinusoidal excitation, including subharmonic vibrations, Hopf bifurcation, symmetry-breaking bifurcations, a series of period-doubling bifurcations and chaos. In past analyses, oscillators with quadratic and/or cubic non-linearities under external excitation or parametric excitation have been studied extensively [2, 6–11]. The non-linearity of a system, through the various system parameters, exhibits a variety of non-linear behaviors including jump phenomenon, multiple attractors, subharmonic vibrations, symmetry breaking-bifurcations, period-doubling bifurcations, crisis and chaos. In addition, a symmetry-breaking bifurcation occurring before a period-doubling bifurcation, and the appearance of chaos amidst a cascade of period-doubling bifurcations, have been observed in driven damped pendulums or Duffing's oscillators by MacDonald and Räty [6, 7]. The behaviors mentioned above occur at the boundaries of stability regions. Therefore, an analysis of instability regions in parametric space is a critical problem.

0022–460X/97/070121 + 17 $25.00/0/sv960695

Recently, a number of non-linear parametrically excited oscillators have been studied in detail by means of approximate analytical methods. Various perturbation techniques are employed in classical weakly non-linear analyses, such as the method of averaging [8, 9] and the method of multiple scales [6, 10]. Szemplińska-Stupnicka [2, 11] has applied the harmonic balance (HB) method to treat strongly non-linear systems well, but its deficiencies are that a set of complex non-linear algebraic equations is formulated and must be solved. Other efficient tools for strongly non-linear systems are the fast Galerkin (FG) method developed by Ling and Wu [12] and the incremental harmonic balance (IHB) method proposed by Lau *et al*. [13–16], which have been successfully applied to various types of non-linear dynamic problems. These two methods can handle strong system non-linearities very well, and provide satisfactory results in a few harmonic terms. These methods are ideally suited to parametric studies for the purpose of seeking parameter diagrams by changing the system parameter in turn. In addition, the multi-variable Floquet theory [17] is applied to analyze the stability of periodic attractors through the moduli of eigenvalues of the associated system monodromy. In this paper, the IHB method is applied to obtain the periodic motions of a system that has strong non-linearity and parametric excitation. Using the multi-variable Floquet theorem, stable periodic attractors and parameter diagrams are presented. Finally, a number of numerical techniques are used to detect the existence of symmetry-breaking bifurcations, period-doubling bifurcations and chaos. The nature of the periodic and chaotic motions are shown in phase plane diagrams, Poincaré maps and average power spectra. Numerical integration results compare very well with those of the IHB. The qualitative bifurcation diagrams, parametric diagrams and quantitative Lyapunov exponents in parametric space are also computed to determine the values of bifurcation points as well as the onset of chaos. Additionally, solution basins of attraction are assessed using modified interpolated cell mapping (MICM) [18]. This method gives more precise and unified results than those from numerical integration by introducing the concept of refined boundary cells.

2. EQUATIONS OF MOTION

We consider the model of a single-rate gyro mounted on a space vehicle, as shown in Figure 1. The gimbal can turn about output X-axis with rotational angle θ. Motion about this axis is resisted by torsional spring and damping torques defined by $k\theta$ and $c\dot{\theta}$

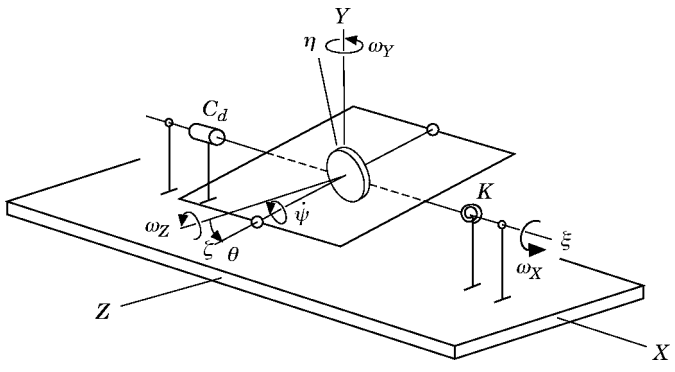

Figure 1. A rate gyro.

respectively. Using Lagrange's equation, the differential equation for the output deflection angle θ of a rate gyro was derived as follows [1]:

$$(A + A_g)\ddot{\theta} + C_d\dot{\theta} + K\theta + Cn_R(\omega_\gamma \cos\theta + \omega_Z \sin\theta) + (A + B_g - C_g)(\omega_Y \cos\theta + \omega_Z \sin\theta)(\omega_Y \sin\theta - \omega_Z \cos\theta) = -(A + A_g)\dot{\omega}_X, \tag{1}$$

where

$$Cn_R = C(\dot{\psi} - \omega_Y \sin\theta + \omega_Z \cos\theta) = \text{constant}, \tag{2}$$

and ω_X, ω_Y and ω_Z denote the angular velocity components of the platform along the output axis X, the input axis Y and the normal axis Z, respectively. A, C and A_g, B_g and C_g denote the moments of inertia of the rotor and gimbal respectively about the gimbal axes ξ, η and ζ.

In this paper, we are interested in the non-linear behavior of dynamical motion when the vehicle undergoes steady rotation about the X-axis, and the harmonic rotation with respect to the Z-axis, i.e., $\dot{\omega}_X = 0$ and $\omega_Z = f \sin\omega_f t$, where f and ω_f are the amplitude and the frequency of the vehicle motion about the Z-axis respectively. Now we let $\omega_Y = 0$ in equation (1), which is divided by $(A + A_g)$. Then the resulting motion of the gimbal can be simplified to

$$\theta'' + 2\alpha\theta' + \theta + \gamma \sin\omega t_1 \sin\theta - \beta(1 - \cos 2\omega t_1)\sin 2\theta = 0, \tag{3}$$

where

$$\theta' = \mathrm{d}\theta/\mathrm{d}t_1, \qquad t_1 = \omega t, \qquad \omega = \frac{\omega_f}{\omega_n}, \qquad \omega_n = \sqrt{K/(A + A_g)},$$

$$\alpha = \frac{C_d}{2(A + A_g)\omega_n}, \qquad \gamma = \frac{Cn_R f}{(A + A_g)\omega_n^2}, \qquad \beta = \frac{(A + B_g - C_g)f^2}{4(A + A_g)\omega_n^2} = \kappa\gamma^2$$

and the values of the above gyro parameters [1] are shown in Appendix I.

If we set $x = \theta$ and $\tau = \omega t_1$, then equation (3) becomes

$$\omega^2\ddot{x} + 2\alpha\omega\dot{x} + x + \gamma \sin\tau \sin x - \beta(1 - \cos 2\tau)\sin 2x = 0, \tag{4}$$

where $\dot{x} = \mathrm{d}x/\mathrm{d}\tau$ and we let $y = \dot{x}$ for plotting.

3. INCREMENTAL HARMONIC BALANCE METHOD

The steady state periodic solutions of equation (4) are obtained by the IHB method, which can deal with strong non-linearity very well and is convenient for computer implementation. Other advantages of this method include its efficient performance of parametric studies and yielding of unstable solutions. The first step in this method is a Newton–Raphson procedure. Let $x_0(\tau)$ denote the current solution of equation (4) corresponding to the excitation parameters ω_0, γ_0 and β_0. A neighboring solution is obtained by adding small increments to the current solution:

$$x = x_0 + \Delta x, \qquad \omega = \omega_0 + \Delta\omega, \qquad \gamma = \gamma_0 + \Delta\gamma, \qquad \beta = \beta_0 + \Delta\beta, \tag{5}$$

where $\Delta\beta = 2\kappa\gamma_0\,\Delta\gamma$.

For a small increment Δx, the non-linear terms $\sin x$ and $\sin 2x$ of equation (4) can be written as first order Taylor expansions:

$$\sin x = \sin x_0 + \cos x_0\,\Delta x, \qquad \sin 2x = \sin 2x_0 + 2\cos 2x_0\,\Delta x. \tag{6}$$

Substituting equations (5) and (6) into equation (4) and ignoring all the non-linear terms, the linearized incremental equation is obtained:

$$\omega_0^2\,\Delta\ddot{x} + 2\alpha\omega_0\,\Delta\dot{x} + (1 + g_1(x_0, \tau))\,\Delta x = R + \Delta\omega F + \Delta\gamma P + \Delta\beta Q, \tag{7}$$

where

$$g_1(x_0, \tau) = \gamma_0 \sin\tau \cos x_0 - 2\beta_0(1 - \cos 2\tau)\cos 2x_0, \tag{8}$$

$$R = -(\omega_0^2\ddot{x}_0 + 2\alpha\omega_0\dot{x}_0 + x_0 + g_2(x_0, \tau)), \tag{9}$$

$$g_2(x_0, \tau) = \gamma_0 \sin\tau \sin x_0 - \beta_0(1 - \cos 2\tau)\sin 2x_0, \tag{10}$$

$$F = -(2\omega_0\ddot{x}_0 + 2\alpha\dot{x}_0), \qquad P = -\sin\tau \sin x_0, \qquad Q = (1 - \cos 2\tau)\sin 2x_0; \tag{11–13}$$

in which R and F are the corrective and imbalance force terms respectively.

The second step of the IHB method is the Galerkin procedure: the approximate periodic solutions $x_0(\tau)$ and $\Delta x(\tau)$ may be expressed as

$$x_0 = \sum_{j=0,1,2,\ldots}^{N} \left(a_{j/q}\cos\frac{j}{q}\tau + b_{j/q}\sin\frac{j}{q}\tau\right),$$

$$\Delta x_0 = \sum_{j=0,1,2,\ldots}^{N} \left(\Delta a_{j/q}\cos\frac{j}{q}\tau + \Delta b_{j/q}\sin\frac{j}{q}\tau\right) \tag{14}$$

for an unsymmetric solution with period $2q\pi$ in terms of τ, and

$$x_0 = \sum_{j=1,3,5,\ldots}^{2N-1} \left(a_{j/q}\cos\frac{j}{q}\tau + b_{j/q}\sin\frac{j}{q}\tau\right),$$

$$\Delta x_0 = \sum_{j=1,3,5,\ldots}^{2N-1} \left(\Delta a_{j/q}\cos\frac{j}{q}\tau + \Delta b_{j/q}\sin\frac{j}{q}\tau\right) \tag{15}$$

for a symmetric solution with period $2q\pi$ in terms of τ; N is the harmonic order to be taken into account and q is the subharmonic order. By applying the Galerkin procedure with Δa_k's and Δb_k's as the generalized co-ordinates, we obtain

$$\int_0^{2q\pi} (\omega_0^2\,\Delta\ddot{x} + 2\alpha\omega_0\Delta\dot{x} + (1+g_1(x_0, \tau))\Delta x)\delta(\Delta x)\,\mathrm{d}\tau$$

$$= \int_0^{2q\pi} (R + \Delta\omega F + \Delta\gamma P + \Delta\beta Q)\delta(\Delta x)\,\mathrm{d}\tau. \tag{16}$$

Substituting equation (14) (or equation (15)) into equation (16) and matching the Δa_k and Δb_k terms, an incremental system of $2N + 1$ (or $2N$) linear equations in terms of the Δa_k's and Δb_k's is obtained in the form of

$$\mathbf{C}\,\Delta\mathbf{a} = \mathbf{R} + \Delta\omega\mathbf{F} + \Delta\gamma\mathbf{P} + \Delta\beta\mathbf{Q}, \tag{17}$$

where

$$\mathbf{a} = [a_{j/q}, b_{j/q}]^{\mathrm{T}},$$

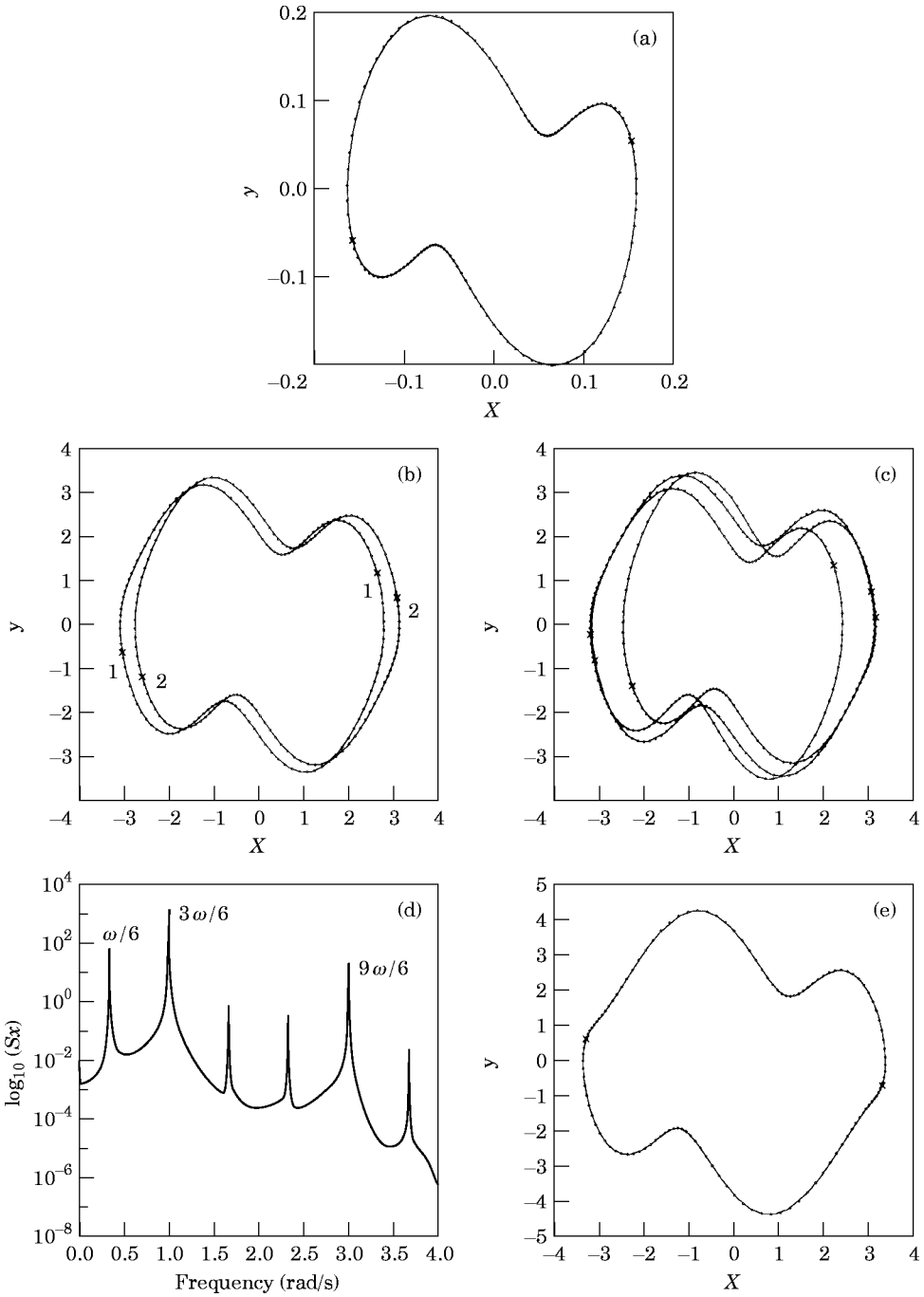

Fig. 2a, b, c, d and e—*Caption overleaf*

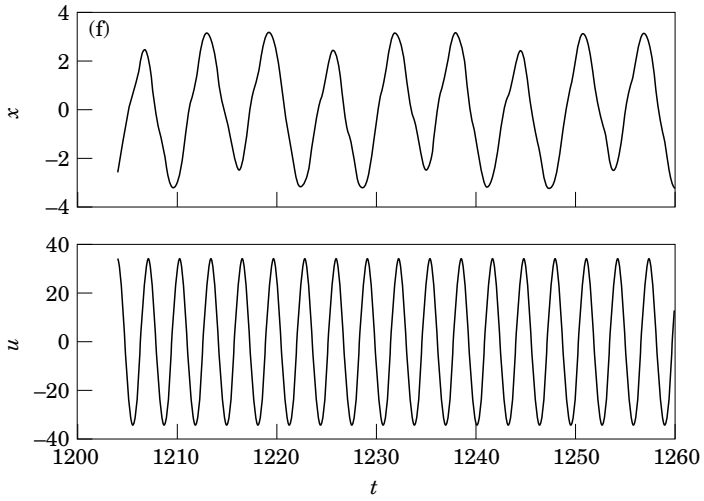

Figure 2. (a) A comparison between IHB (●●●●) and numerical integration (—) of a symmetry period-2T cycle for $f = 15{\cdot}45$. (b) A comparison between IHB (●●●●) and numerical integration (—) of a dual period-2T cycle for $f = 32{\cdot}83$. (c) A comparison between IHB (●●●●) and numerical integration (—) of a symmetry period-6T cycle for $f = 34{\cdot}4$. (d) An average power spectrum of Figure 2(c). (e) A comparison between IHB (●●●●) and numerical integration (—) of a symmetry period-2T cycle for $f = 45$. (f) The time histories of the periodic solution (x) and the external excitation ($u = f \sin \omega\tau$) of Figure 2(c).

$$\Delta \mathbf{a} = [\Delta a_{j/q}, \Delta b_{j/q}]^{\mathrm{T}}, \qquad j = \begin{cases} 0, 1, 2, \ldots, N & \text{for an unsymmetric solution,} \\ 1, 3, \ldots, 2N-1 & \text{for a symmetric solution;} \end{cases} \tag{18}$$

$$\mathbf{C} = \begin{bmatrix} [\mathbf{C}_1]_{ij} & [\mathbf{C}_{12}]_{ij} \\ [\mathbf{C}_{21}]_{ij} & [\mathbf{C}_2]_{ij} \end{bmatrix}, \qquad \mathbf{R} = \begin{bmatrix} R_{1i} \\ R_{2i} \end{bmatrix}, \qquad \mathbf{F} = \begin{bmatrix} F_{1i} \\ F_{2i} \end{bmatrix}, \qquad \mathbf{P} = \begin{bmatrix} P_{1i} \\ P_{2i} \end{bmatrix}, \qquad \mathbf{Q} = \begin{bmatrix} Q_{1i} \\ Q_{2i} \end{bmatrix}. \tag{19–23}$$

The expressions **C**, **R**, **F**, **P** and **Q** are given in detail in Appendix II.

4. STABILITY ANALYSIS

From the previous procedure, the qT-period steady state solution $x_0(\tau)$ has been determined and its local stability is investigated by considering the following perturbation solution:

$$x = x_0 + \delta x. \tag{24}$$

Inserting equation (24) into equation (4), and ignoring the higher order terms in δx, we obtain a linear variational equation with periodic coefficients in the following form:

$$\omega^2 \delta\ddot{x} + 2\alpha\omega\delta\dot{x} + (1 + g_1(x_0, \tau))\delta x = 0. \tag{25}$$

Equation (25) can then be arranged in matrix form as

$$\dot{\mathbf{X}} = \mathbf{A}(\tau)\mathbf{X}, \tag{26}$$

where

$$\mathbf{X} = [\delta x, \delta\dot{x}]^{\mathrm{T}}, \qquad \mathbf{A}(\tau) = \begin{bmatrix} 0 & 1 \\ A_{21} & -2\alpha/\omega \end{bmatrix}, \qquad A_{21} = -(1 + g_1(x_0, \tau))/\omega^2. \tag{27}$$

Since x_0 is a periodic function of time τ with a period $T_q = 2q\pi$, the coefficient matrix $\mathbf{A}(\tau)$ has the same period T_q; i.e., $\mathbf{A}(\tau + T_q) = \mathbf{A}(\tau)$. The stability of a linear perodic system is analyzed by the multi-variable Floquet–Lyapunov theory with an efficient numerical scheme for computing the transition matrix at the end of one period, $\mathbf{\Phi}(T_q, 0)$ [17]. Here, the approximate transiton matrix $\mathbf{\Phi}(T_q, 0)$ is given in the following form:

$$\mathbf{\Phi}(T_q, 0) = \prod_{i=1}^{N_k} \left(\mathbf{I} + \sum_{j=1}^{N_j} \frac{(\Delta_i B_i)^j}{j!} \right) \tag{28}$$

$$\mathbf{B}_k = \frac{1}{\Delta_k} \int_{\tau_{k-1}}^{\tau_k} \mathbf{A}(\zeta)\, \mathrm{d}\zeta, \tag{29}$$

where N_k is the number of intervals in each period T; N_j is the number of terms in the approximation of the constant matrix B_i exponential; the kth interval is denoted by τ_k, and its size by $\Delta_k = \tau_k - \tau_{k-1}$; and in the kth interval the periodic coefficient matrix $\mathbf{A}(\tau)$ is replaced by a constant matrix $\mathbf{B}_k$.

The eigenvalues of the monodromy matrix $\mathbf{\Phi}(T_q, 0)$ are also called the Floquet multipliers (ρ_1, ρ_2) and can determine the stability of a steady state solution. If all of the moduli of the eigenvalues ρ_k are smaller than unity, the solution is stable. If the moduli of one of the eigenvalues ρ_k is larger than unity, the solution is unstable. Bifurcation occurs when an eigenvalue ρ_k passes through the unit circle.

5. NUMERICAL SIMULATIONS AND DISCUSSION

Varying the system parameter f, the system results obtained by the IHB method were compared with the results obtained by numerical integration in the phase planes. There

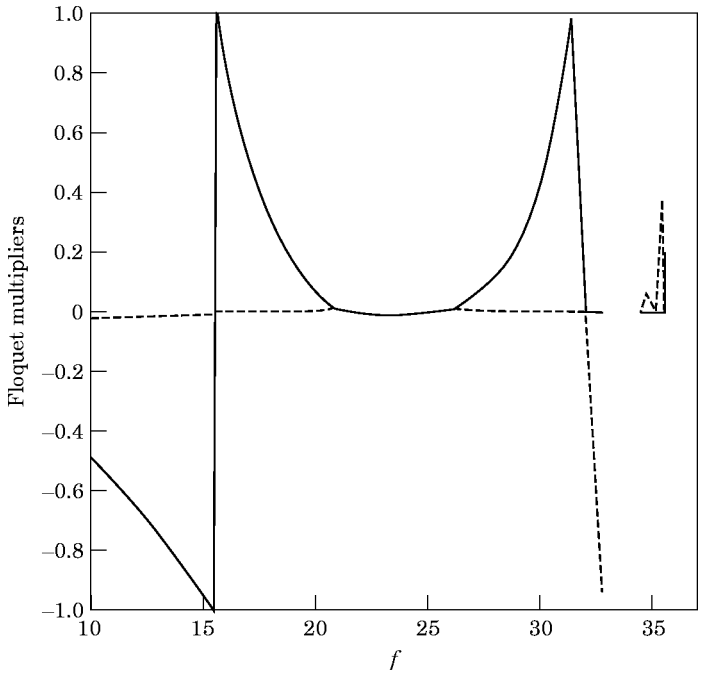

Figure 3. Floquet multipliers as a function of f.

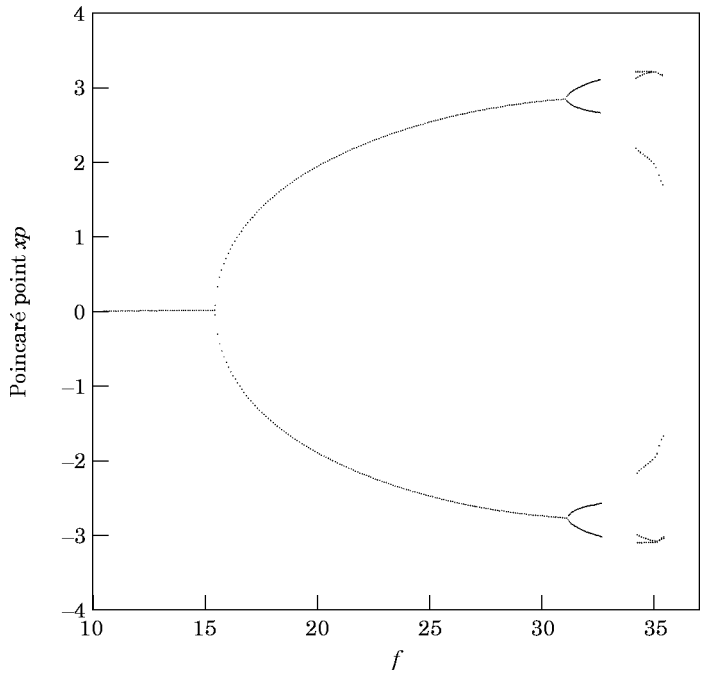

Figure 4. The response in a Poincaré section by IHB.

was good agreement between IHB and numerical integration as shown in Figures 2(a)–(e), where the symbols "●" and "×" indicate the results obtained by the IHB method and one period T of sinusoidal motion, respectively. The attractor of the system is a hyperbolic

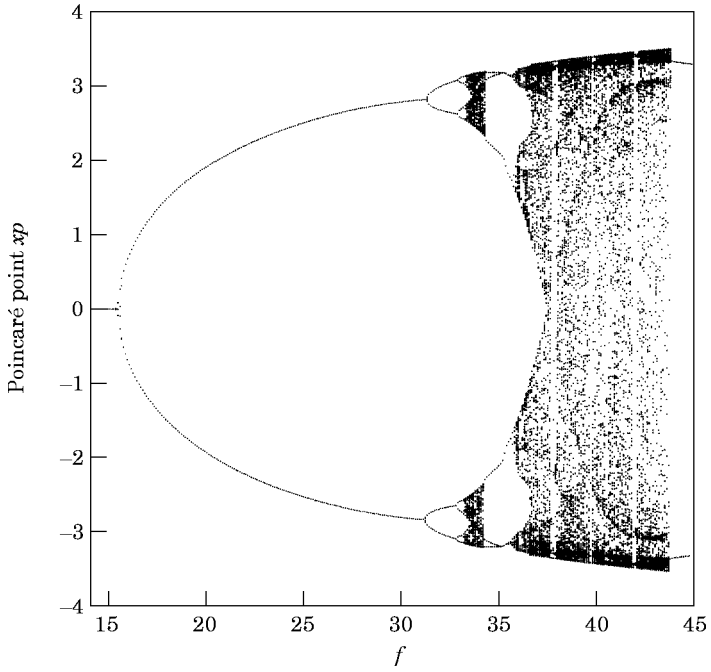

Figure 5. The bifurcation diagram.

TABLE 1

Limit points for various parametric studies

Parametric study	Lyapunov diagram	Bifurcation diagram		Floquet diagram	Floquet multiplier
Figure	Figure 9	Figure 5	Figure 4	Figure 3	
Method	RK4			IHB	
Parameter	f				ρ
A	15·57	15·45	15·43	15·43	0·998
B	31·24	31·25	31·35	31·33	0·982
C	32·89	32·95	32·85	32·8	0·939
D	33·34	33·35	—	—	—
E	34·33	34·35	34·35	34·35	—
F	35·85	36·00	35·7	35·7	—
G	43·88	43·85	—	—	—

A: a fixed point bifurcates to a symmetry period-2T cycle. B: a symmetry period-2T bifurcates to an asymmetry period-2T cycle. C: an asymmetry period-2T bifurcates to an asymmetry period-4T cycle. D: the first chaotic attractor appears. E: a chaotic attractor disappears and a symmetry period-6T cycle appears. F: a symmetry period-6 T cycle disappears and a chaotic attractor appears. G: a chaotic attractor disappears and a symmetry period-2T cycle appears.

fixed point at the origin before the parameter $f = 15{\cdot}43$. In the neighborhood of $f = 15{\cdot}43$, one of the Floquet multipliers leaves the unit circle through -1 for the fixed point and jumps to the $+1$ boundary of the unit circle for the periodic solution, as shown in Figure 3. Hopf bifurcation of an equilibrium point and a period-2T stable symmetric cycle occurring

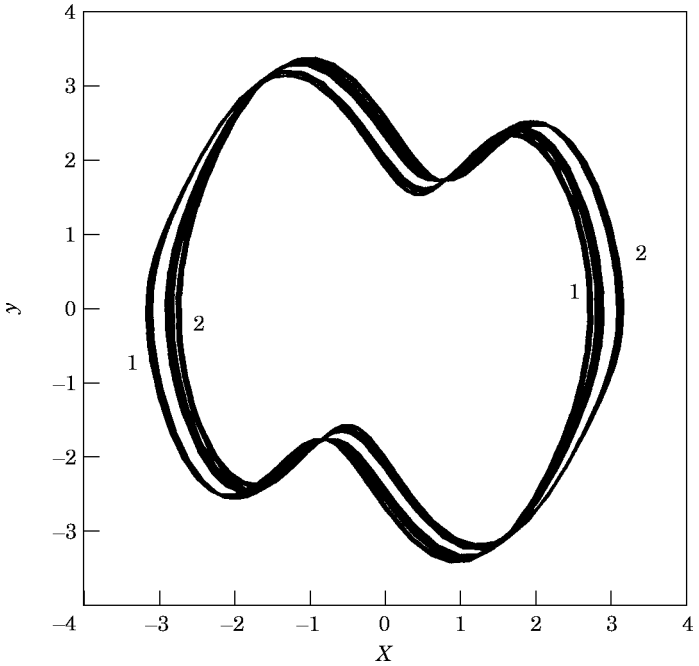

Figure 6. Two inverse chaotic attractors for $f = 33{\cdot}4$.

are shown in Figure 2(a), where $T = 2\pi/\omega$. A system with a symmetric non-linear function, i.e., $g_1(x(\tau), \tau) = -g_1(-x(\tau), \tau)$, can undergo either a symmetry-breaking bifurcation at the Floquet multiplier $\rho = +1$ for the symmetric solution of the system or a period-doubling bifurcation at the Floquet multiplier $\rho = -1$ for the asymmetric solution of the system. When $f = 31{\cdot}35$, a multiplier touches the $+1$ boundary of the unit circle and a symmetry-breaking bifurcation occurs. After this bifurcation, the original stable period-$2T$ attractor becomes unstable, and a pair of stable period-$2T$ attractors arise and invert each other, as shown in Figure 2(b) where $f = 32{\cdot}83$, with nine harmonic terms in the IHB method. As the parameter f increases further across 32·95, the multiplier leaves the unit circle through the -1 boundary and a stable periodic orbit appears with double the period of the original orbit, thereby indicating a period-doubling (flip) bifurcation. When the parameter is increased, a cascade of flip bifurcations occurs and leads to the onset of chaos. At $f = 34{\cdot}4$, the chaotic attractor abruptly disappears and a period-$6T$ symmetric orbit appears, as shown in the phase plane and average power spectrum (Figures 2(c) and (d)), from which 15 odd harmonic terms are employed in the computation. Indeed, for the large parameter $f = 45$, an accurate period-$2T$ attractor is also obtained with only seven odd harmonic terms considered, as shown in Figure 2(e). The above-mentioned phase planes show that the attractors obtained by the IHB method with a few harmonic terms retained are in excellent agreement with those obtained by numerical integration. Additionally, the time histories of periodic solutions of Figure 2(c), as well as the external excitation, are presented in Figure 2(f).

The different types of bifurcations can be verified by calculating the Floquet multipliers of the monodromy matrix as a function of the parameter f, as shown in Figure 3. To investigate bifurcation further, a Poincaré plane was used to display the bifurcation diagram in Figure 4, which shows Poincaré fixed points x_p plotted against the system parameter f. The Hopf bifurcation, symmetry-breaking bifurcation and period-doubling bifurcation are clearly shown. This bifurcation diagram also shows good agreement

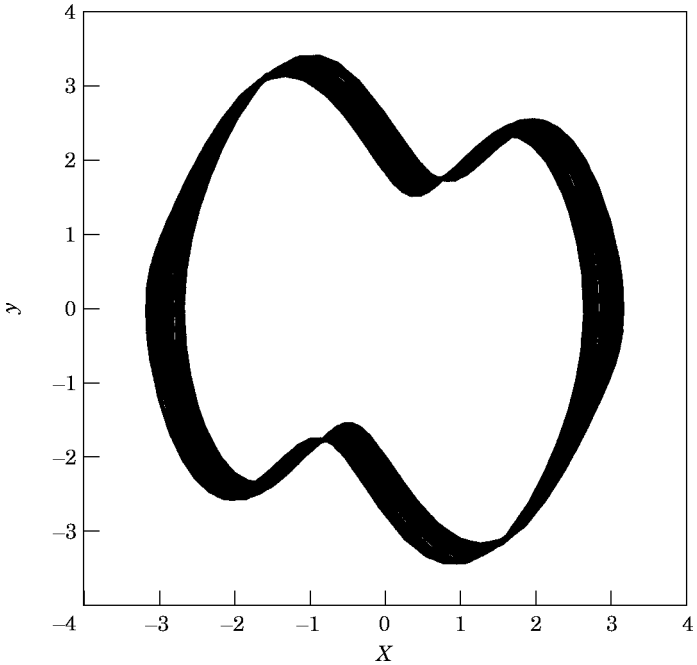

Figure 7. A chaotic attractor in conjunction with two inverse chaotic attractors for $f = 33{\cdot}7$.

between the IHB method and numerical integration. The IHB method is ideally suited to parametric studies for obtaining solution diagrams, and can find all possible solutions, including unstable solutions which cannot be obtained by numerical integration. In addition, the method can obtain accurate results directly in the frequency domain. However, to obtain the higher qT-period solutions, a number of harmonics must be considered and a set of good initial conditions needs to be specified that will converge to the predicted stable attractors. Another disadvantage of the IHB method is that the computation time required increases geometrically with the number of harmonic terms considered. Hence, the higher periodic and chaotic attractors were analyzed by fourth order Runge–Kutta numerical integration. The results are shown in a number of phase plane diagrams, Poincaré maps, average power spectra, bifurcations and Lyapunov exponents.

As the system parameter f is gradually increased through the parametric space, the bifurcation diagram obtained shows different types of bifurcations and chaos (see Figure 5). The values of the main limit points are shown in Table 1. As observed earlier, the Hopf bifurcation at $f = 15{\cdot}45$, the symmetry-breaking bifurcation at $f = 31{\cdot}25$ and the

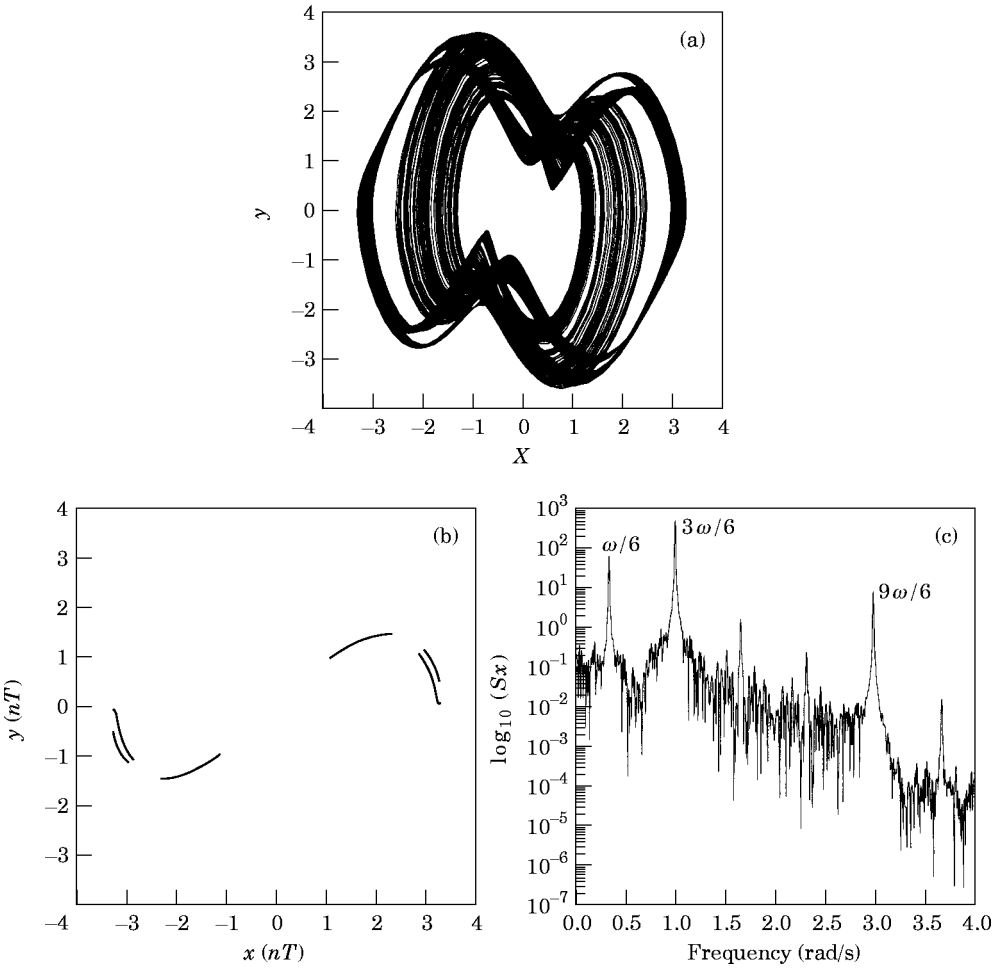

Figure 8. A symmetric chaotic attractor plotted: (a) in the phase plane and (b) on Poincaré maps. (c) The average power spectrum for $f = 36{\cdot}5$.

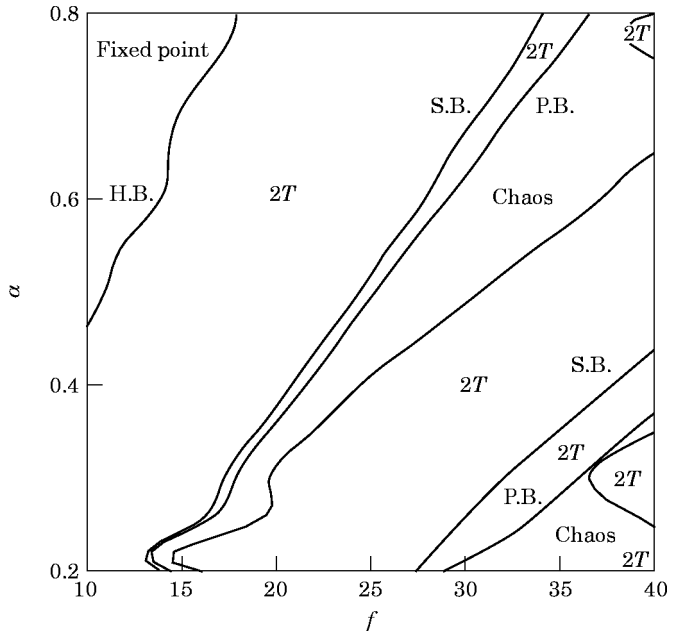

Figure 9. The parametric diagram in the f–α plane; $\omega = 2{\cdot}0$.

period-doubling bifurcation at $f = 32{\cdot}95$ are also predicted accurately by the IHB method. To investigate the periodic and chaotic motions in the bifurcation diagram further, the phase planes, Poincaré maps and power spectra are used. After a cascade of period-doubling bifurcations, the dual response becomes chaotic rather than periodic for $f = 33{\cdot}4$, as shown in Figure 6. When $f = 33{\cdot}7$, conjunction of the two inverse chaotic

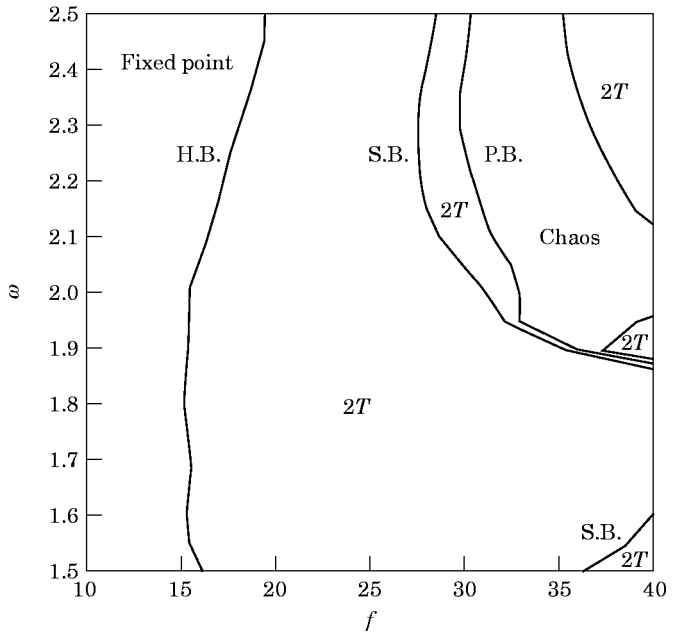

Figure 10. The parametric diagram in the f–ω plane; $\alpha = 0{\cdot}7$.

attractors creates a larger attractor, as shown in Figure 7. With the parameter increased, a large amplitude chaotic motion appears in the phase plane, Poincaré map and power spectrum, as shown in Figure 8, where $f = 36{\cdot}5$. In addition, parametric diagrams were constructed in which the boundaries of Hopf bifurcation (H.B.), symmetry-breaking bifurcation (S.B.) and period-doubling bifurcation (P.B.) were shown, as in Figures 9 and 10. The symbol $2T$ refers to a limit cycle of period-$2T$, where $T = 2\pi/\omega$ and the fixed point is at the origin.

To confirm the chaotic dynamics, a qualitative and quantitative Lyapunov exponent spectrum was performed. The algorithm for calculating the Lyapunov exponents was developed by Wolf *et al*. [19]. A spectrum of the largest Lyapunov exponent as a function of the parameter f is shown in Figure 11. As one of the Lyapunov exponent is positive, the motion is characterized as chaotic. When at least one Lyapunov exponent $\lambda_1 = 0$ exists, the motions are not stationary. For periodic motions, the Lyapunov exponents are non-positive and include only one zero Lyapunov exponent, while one negative exponent becomes zero when one type of periodic motion bifurcates to another.

In this case the sum of all three Lyapunov exponents, $\lambda_1 + \lambda_2 + \lambda_3 = -1{\cdot}399$, is equivalent to the negative damping coefficient of the system, independent of position and time. For $f = 33{\cdot}7$ the Lyapunov exponents were found to be $\lambda_1 = 0{\cdot}119$, $\lambda_2 = 0$ and $\lambda_3 = -1{\cdot}518$, and the Lyapunov dimension $d_L = 2{\cdot}0784$ was also calculated using the relation proposed by Frederickson *et al*. [20]:

$$d_L = j + \sum_{i=1}^{j} \lambda_i / |\lambda_{j+1}|,$$

where λ_1 is the largest Lyapunov exponent and j is the index of the smallest non-negative Lyapunov exponents. From the above discussion, it is evident that Lyapunov exponents are a measure of the fractal geometry of the attractor and the property of sensitivity dependence on initial conditions.

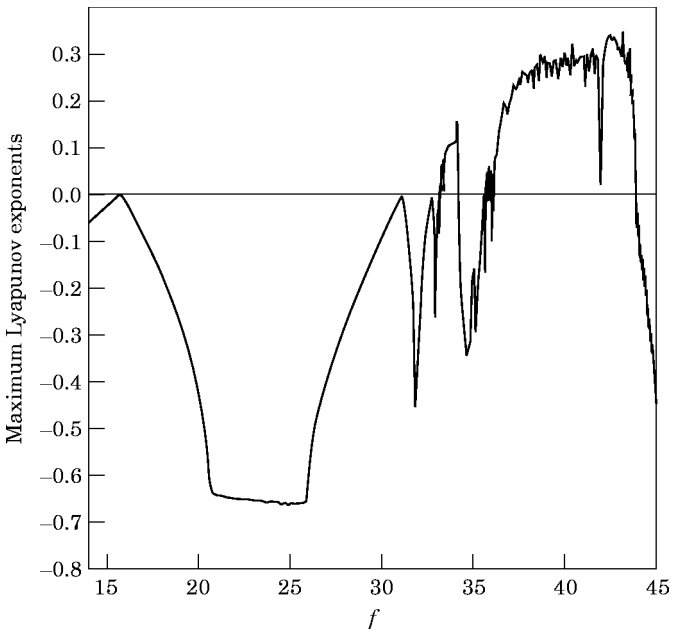

Figure 11. The largest Lyapunov exponents as a function of f.

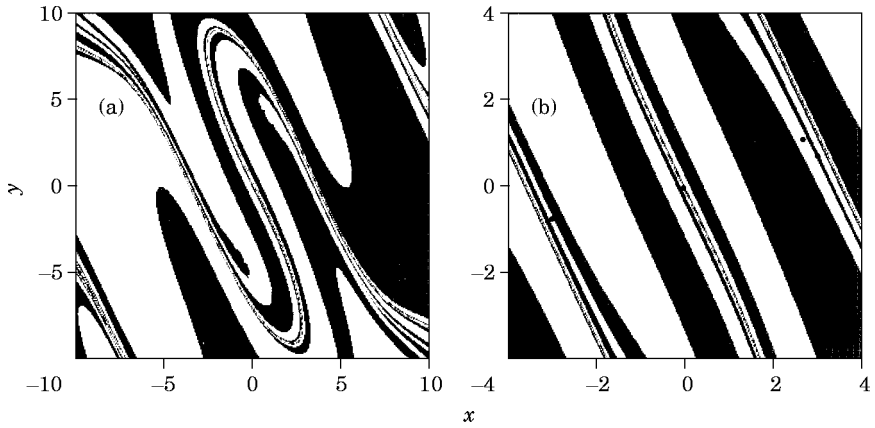

Figure 12. The attracting basins of two inverse period-2T attractors with a magnification sequence for $f = 32{\cdot}5$.

It is well known that attractors and basins of attraction may be obtained in regions of interest using cell mapping techniques. Various cell mapping algorithm exists that allow efficient evaluation of attracting basins. Here the modified interpolated cell mapping (MICM) algorithm [18] is considered to identify the periodic attractor basins of attraction and their dual attractors, for $f = 32$, which corresponds to the period-2T. In Figure 12, the basins of attraction of two inverse attractors are inverse to each other with respect to the shaded and unshaded regions because the non-linearity of the system is symmetric. The initial conditions in each region generate orbits that generally approach a period-2T attractor (labeled by two dots in the figure). Another dot $(x, \dot{x}) = (0, 0)$ on the basin boundary is the saddle. In fact, the saddle manifold of the saddle is the basin boundary. For different diagrams of previous parametric studies, the limit points are consistent with each other, as shown in Table 1.

6. CONCLUSIONS

In this paper, a single-axis rate gyro with sinusoidal velocity about its spin axis exhibits the non-linear characteristic of both sine function and parametric excitations when the parameter is varied. A variety of parametric studies were performed to analyze the behavior of bifurcations and chaos using the IHB method and numerical integration. In the parametric studies, the periodic attractors can be clearly seen in these diagrams and their stability was analyzed by applying the Floquet multi-variable theory. The behaviors of a symmetry-breaking precursor to period-doubling bifurcations and a cascade of period-doubling routes to chaos occurred in this system. The chaotic motion was confirmed by the Poincaré map, a continuous board power spectral diagram and the existence of a positive Lyapunov exponent. The attracting basins of the periodic responses were also assessed by MICM, which provided information about large scale stability regions.

ACKNOWLEDGMENTS

The authors wish to thank the referees for their valuable and helpful comments on this paper. The authors are grateful to the National Science Council, Republic of China, for supporting this research under grant NSC 84-2212-E-009-021.

REFERENCES

1. A. H. Nayfeh and D. T. Mook 1979 *Nonlinear Oscillations*. New York: John Wiley. See Chapters 4 and 5.
2. W. Szemplińska-Stupnicka, R. H. Plaut and J.-C. Hsieh 1989 *Transactions of the American Society of Mechanical Engineers*, *Journal of Applied Mechanics* **56**, 947–952. Period doubling and chaos in unsymmetric structures under parametric excitation.
3. S. N. Singh 1984 *IEEE Transactions on Aerospace and Electronic Systems* **AES-20**, 119–127. Gyro motion boundedness under uncertain vehicle spin and acceleration.
4. Z. M. Ge and C. J. Chen 1992 *AIAA Journal of Guidance*, *Control*, *and Dynamics* **15**, 1034–1036. Stability of a rate gyro.
5. J. Guckenheimer and P. Holmes 1986 *Nonlinear Oscillations*, *Dynamical Systems and Bifurcation of Vector Fields*. New York; Springer-Verlag. See Chapters 4–7.
6. A. H. MacDonald and M. Plischke 1983 *Physical Review B* **27**, 201–211. Study of the driven damped pendulum: application to Josephson junctions and charge-density – wave systems.
7. R. Räty, J. Von Boehm and H. M. Isomäki 1984 *Physics Letters* **103A**, 289–292. Absence of inversion-symmetric limit cycles of even periods and the chaotic motion of Duffing's oscillator.
8. J. A. Sanders and F. Verhulst 1985 *Averaging Methods in Nonlinear Dynamics*. New York: Springer-Verlag. See Chapter 3.
9. K. Yagasaki, M. Sakata and K. Kimura 1990 *Transactions of the American Society of Mechanical Engineers*, *Journal of Applied Mechanics* **57**, 209–217. Dynamics of a weakly nonlinear system subjected to combined parametric and external excitation.
10. N. E. Sanchez and A. H. Nayfeh 1990 *International Journal of Non-linear Mechanics* **25**, 163–176. Prediction of bifurcations in a parametrically excited Duffing oscillator.
11. W. Szemplińska-Stupnicka 1987 *Journal of Sound and Vibration* **113**, 155–172. Secondary resonances and approximate models of routes to chaotic motions in non-linear oscillations.
12. F. H. Ling and X. X. Wu 1987 *International Journal of Non-linear Mechanics* **22**, 89–98. Fast Galerkin method and its application to determine periodic solution of non-linear oscillators.
13. S. L. Lau, Y. K. Cheung and S. Y. Wu 1982 *Transactions of the American Society of Mechanical Engineers*, *Journal of Applied Mechanics* **49**, 849–853. A variable parameter incrementation method for dynamic instability of linear and nonlinear elastic systems.
14. Y. K. Cheung, S. H. Chen and S. L. Lau 1990 *Journal of Sound and Vibration* **140**, 273–286. Application of the incremental harmonic balance method to cubic non-linearity systems.
15. L. Lau and S. W. Yuen 1991 *Computer Methods in Applied Mechanics and Engineering* **91**, 1109–1121. The Hopf bifurcation and limit cycle by the incremental harmonic balance method.
16. S. L. Lau and S. W. Yuen 1993 *Journal of Sound and Vibration* **167**, 303–316. Solution diagram of non-linear dynamic systems by the IHB method.
17. P. Friedmann, C. E. Hammond and T. H. Woo 1977 *International Journal of Numerical Methods in Engineering* **11**, 1117–1136. Efficient numerical treatment of periodic systems with application to stability problems.
18. Z. M. Ge and S. C. Lee 1997 *Journal of Sound and Vibration*, **199,** 189–206. A modified interpolated cell mapping method.
19. A. Wolf, J. B. Swift, H. L. Swinney and J. A. Vastano 1985 *Physica* **16D**, 285–317. Determining Lyapunov exponents from a time series.
20. P. Frederickson, J. L. Kaplan, E. D. Yorke and J. A. Yorke 1983 *Journal of Differential Equations* **49**, 185–207. The Lyapunov dimension of strange attractors.

APPENDIX I

The values of the gyro parameters are as follows:

$$(A + A_g) = 54 \text{ dyne cm s}^2, \qquad Cn_R = 10{\cdot}8 \times 10^4 \text{ dyne cm s},$$

$$K = 54 \times 10^4 \text{ dyne cm rad}^{-1}, \qquad C_d = 7560 \text{ dyne cm rad}^{-1} \text{ s},$$

$$\frac{C_d}{(A + A_g)} = 140 \text{ rad}^{-1} \text{ s}^{-1}, \qquad \frac{K}{(A + A_g)} = 10^4 \text{ rad}^{-1} \text{ s}^{-2},$$

$$\frac{Cn_R}{(A+A_g)} = 2000\ \mathrm{s}^{-1}, \qquad \frac{(A+B_g-C_g)}{(A+A_g)} = 1,$$

$$\omega_n = 100\ \mathrm{rad\ s}^{-1}, \qquad \omega = \frac{\omega_f}{\omega_n} = 2, \qquad \alpha = 0{\cdot}7, \quad \beta = 2{\cdot}5 \times 10^{-5} f^2, \qquad \gamma = 0{\cdot}2f.$$

APPENDIX II

The elements of matrix **C** are as follows:

$$[\mathbf{C}_1]_{ij} = \mu_j \delta_{ij} q\pi \left(1 - \left(\frac{j\omega_0}{q}\right)^2\right) + [\mathbf{C}_1]_{ij}^{NL}, \qquad i, j = 0, 1, \ldots, N;$$

$$[\mathbf{C}_{12}]_{ij} = 2\delta_{ij} q\pi \left(\frac{j\omega_0}{q}\right) + [\mathbf{C}_{12}]_{ij}^{NL}, \qquad i = 0, 1, \ldots, N, \quad j = 1, \ldots N;$$

$$[\mathbf{C}_{12}]_{ij} = -2\delta_{ij} q\pi \left(\frac{j\omega_0}{q}\right) + [\mathbf{C}_{21}]_{ij}^{NL}, \qquad i = 1, \ldots, N, \quad j = 0, 1, \ldots N;$$

$$[\mathbf{C}_2]_{ij} = \delta_{ij} q\pi \left(1 - \left(\frac{j\omega_0}{q}\right)^2\right) + [\mathbf{C}_2]_{ij}^{NL}, \qquad i, j = 1, \ldots, N,$$

where

$$\mu_j = \begin{cases} 2 & \text{for } j = 0, \\ 1 & \text{for } j \neq 0, \end{cases} \qquad \delta_{ij} = \begin{cases} 1 & \text{for } i = j, \\ 0 & \text{for } i \neq j, \end{cases}$$

$$[\mathbf{C}_1]_{ij}^{NL} = \int_0^{2q\pi} g_1(x_0, \tau) \cos\frac{i\tau}{q} \cos\frac{j\tau}{q}\, \mathrm{d}\tau,$$

$$[\mathbf{C}_{12}]_{ij}^{NL} = \int_0^{2q\pi} g_1(x_0, \tau) \cos\frac{i\tau}{q} \sin\frac{j\tau}{q}\, \mathrm{d}\tau,$$

$$[\mathbf{C}_{21}]_{ij}^{NL} = \int_0^{2q\pi} g_1(x_0, \tau) \sin\frac{i\tau}{q} \cos\frac{j\tau}{q}\, \mathrm{d}\tau,$$

and

$$[\mathbf{C}_2]_{ij}^{NL} = \int_0^{2q\pi} g_1(x_0, \tau) \sin\frac{i\tau}{q} \sin\frac{j\tau}{q}\, \mathrm{d}\tau.$$

The elements of vectors **R**, **F**, **P** and **Q** are as follows:

$$\mathbf{R}_{1i} = -\mu_i \left(\left(1 - \left(\frac{i\omega_0}{q}\right)^2\right) a_i + 2\alpha \left(\frac{i\omega_0}{q}\right) b_i \right) q\pi + R_{1i}^{NL}, \qquad i = 0, 1, \ldots, N;$$

$$\mathbf{R}_{2i} = -\left(\left(1-\left(\frac{i\omega_0}{q}\right)^2\right)b_i - 2\alpha\left(\frac{i\omega_0}{q}\right)a_i\right)q\pi + R_{2i}^{NL}, \qquad i = 1, 2, \ldots, N;$$

$$\mathbf{F}_{1i} = 2q\pi\mu_i\left(\omega_0\left(\frac{i}{q}\right)^2 a_i - \alpha\frac{i}{q}b_i\right), \qquad i = 0, 1, \ldots, N;$$

$$\mathbf{F}_{2i} = 2q\pi\left(\omega_0\left(\frac{i}{q}\right)^2 b_i + \alpha\frac{i}{q}a_i\right), \qquad i = 1, 2, \ldots, N;$$

$$\begin{Bmatrix}\mathbf{P}_{1i}\\ \mathbf{P}_{2i}\end{Bmatrix} = \int_0^{2q\pi} -\sin x_0 \begin{Bmatrix}\cos(i\pi/q)\\ \sin(i\pi/q)\end{Bmatrix} \mathrm{d}\tau;$$

$$\begin{Bmatrix}\mathbf{Q}_{1i}\\ \mathbf{Q}_{2i}\end{Bmatrix} = \int_0^{2q\pi} (1-\cos\tau)\sin 2x_0 \begin{Bmatrix}\cos(i\pi/q)\\ \sin(i\pi/q)\end{Bmatrix} \mathrm{d}\tau;$$

where

$$\mathbf{R}_{1i}^{NL} = -\int_0^{2q\pi} g_2(x_0, \tau)\cos\frac{i\tau}{q}\,\mathrm{d}\tau \qquad \text{and} \qquad \mathbf{R}_{2i}^{NL} = -\int_0^{2q\pi} g_2(x_0, \tau)\sin\frac{i\tau}{q}\,\mathrm{d}\tau.$$